IEEE Access
Multidisciplinary | Rapid Review | Open Access Journal

Received March 31, 2021, accepted April 11, 2021, date of publication April 15, 2021, date of current version April 27, 2021.

Digital Object Identifier 10.1109/ACCESS.2021.3073470

A Multi-Tier Inspection Queueing System With Finite Capacity for Differentiated Border Control Measures

CHIA-HUNG WANG[1,2], (Member, IEEE), YU-TIN CHEN[3], AND XIAOJING WU[4]

[1]College of Computer Science and Mathematics, Fujian University of Technology, Fuzhou 350118, China
[2]Fujian Provincial Key Laboratory of Big Data Mining and Applications, Fujian University of Technology, Fuzhou 350118, China
[3]Hengzen Technology Company Ltd., Taipei 11677, Taiwan
[4]College of Electronics, Electrical Engineering and Physics, Fujian University of Technology, Fuzhou 350118, China

Corresponding author: Yu-Tin Chen (wytchen@gmail.com)

ABSTRACT Both uniform quarantine and isolation measures, due to the COVID-19 pandemic, have brought forth unprecedented and severe socio-economic impacts. For the global post-COVID economic recovery, it is of great significance to explore scientific ways to reopen the borders with consideration of both risk and efficiency. With the development of international travel health certificate or digital travel pass, differentiated inspection and quarantine measures can be implemented to accelerate the recovery of international travel. In this paper, we study a multi-tier inspection queueing system with finite capacity based on a differentiated level of risk classification. A queueing analysis is conducted for the stochastic process of inspecting cross-border travelers under differentiated service for inspection and quarantine. Besides, we develop a computing method to determine the steady-state probability and several performance indices of the proposed queueing system, and an illustrative example is also set to introduce a step-by-step process for the method. Furthermore, we figure out the relationship between the model parameters and system performance of interest by means of a series of numerical experiments. In the data analysis, we also illustrate the monotonic and concave effects on the system performance, which can provide a visualized understanding of the trade-off between safety and efficiency in the studied multi-server queueing system with hierarchical inspection channels and finite capacity. Our findings can reveal some managerial insight into the border control problems, which could reconcile the efficiency with safety in the current epidemic prevention and control tasks.

INDEX TERMS Queueing model, multi-server queue, operations management, data analysis, risk-based strategy, system analysis and design, performance evaluation, border control, inspection and quarantine measures, COVID-19 pandemic.

I. INTRODUCTION

The ongoing novel coronavirus (COVID-19) epidemic has already caused a global pandemic [1]–[3]. As of March 14, 2021, there are 223 countries and regions with confirmed cases, while the cumulative numbers of COVID-19 infected cases and confirmed deaths increasingly mount to 119,030,459 and 2,640,349 according to the statistical data from World Health Organization (WHO) [4]. In order to avoid the spread of epidemic, most countries and regions have invested resources to carry out epidemic prevention and control tasks related to border control measures [5].

The advent of COVID-19 pandemic has brought forth unprecedented and severe socio-economic impacts, taking cross-border transportation cancelation as an example. The number of travelers at security checkpoints in Year 2020 was over 70% lower than the statistics in the prior year [6]. The transportation and tourism industries account for a large proportion of Gross Domestic Product (GDP), and the losses of these two due to the epidemic have a great impact on the national economy. Thus, governments worldwide are struggling to find ingenious ways to somewhat restore the flow

The associate editor coordinating the review of this manuscript and approving it for publication was Md. Asaduzzaman.

streams associated with cross-border movement of people and goods.

Some countries and organizations have begun to study reopening their borders without isolation measures. For example, the International Air Transport Association (IATA) announced in December 2020 that it was going to create an ''IATA Travel Pass'', allowing travelers to store and manage personal health information or certifications for COVID-19 tests/vaccines [7]. The IATA Travel Pass is a mobile application, which aims to help travelers check the entry quarantine requirements for all destinations before their departure and make response, according to the border control regulations. Besides, Air France has started testing a health passport system from March 2021, for passengers on selected flights, who obligate to show proof of vaccination or negative COVID-19 test results. The passport will work through an app called ICC AOKpass, which will be presented on the plane.

For reopening international travel, China has launched the Chinese version of travel health certificate. On March 8, 2021, China made an available digital passport for citizens, ''International Travel Health Certificate'', certifying the health status of travelers. The official data in the Chinese version of International Travel Health Certificate is provided by the National Health Commission of the People's Republic of China, including Nationality, Passport No., Name, Result of Nucleic Acid Test, Nucleic Acid Testing Institution, Date of Nucleic Acid Test, Result of Serum IgG Antibody Test, Serum IgG Antibody Testing Institution, Date of Serum IgG Antibody Test, and some data related to COVID-19 vaccination, etc. Meanwhile, in the European Union, the idea of a ''Green Passport'' is going to be presented by the European Commission in March 2021. Besides that, the Unite States of America is considering the launch of similar travel health certificate/passport.

With the development of all kinds of COVID-19 health certificates or digital health passports, there will be an opportunity to accelerate the recovery of international travelling. We can carry out the risk assessment by classification or stratification for different types of international travelers with different risk levels [8]–[15]. Cross-border travelers can upload personal health information to those databases, which could label differentiated risk classes and accurately notify border control personnel whether they are qualified for cross-border travel or not [16]–[21]. During the post-COVID economic recovery, these international travel health certificates/passports could help reopen borders further.

Queueing theory has been applied extensively to estimate the performance of stochastic systems [22]–[25]. In the present work, we have applied queueing analysis to a multi-tier inspection system based on differentiated levels of risk classification. A multi-server queueing model with finite capacity will be developed in this paper in order to investigate the stochastic process of differentiated service for inspection and quarantine measures. Furthermore, we are going to derive a computing method for the studied multi-server queueing system with hierarchical inspection channels and finite capacity, and determine the system performance of interest. Besides, the proposed queueing model and computing method will be demonstrated by means of a series of numerical examples. We will also conduct a sensitivity analysis of the system performance as the model parameters are varied.

In this paper, we are going to investigate a managerial problem for the border-crossing queueing process with hierarchical inspection channels. The proposed queueing analysis is of great significance to clarify the risk management goals that aim to effectively and efficiently optimize the tight resource for border control [26]–[28]. Our findings can provide some managerial insight into the border control problems that reconcile the efficiency with safety in the current epidemic prevention and control tasks, especially when attempting to implement the strategy of accurately classified or differentiated prevention and control, and dredging the bottleneck points at borders for passenger flow or container logistics. Our research work could help the decision makers improve the customs clearance inspection and quarantine mechanism, under consideration of both strengthening supervision and optimizing service.

The structure of the present paper is organized as follows. In Section II, we will introduce the problem definitions and a multi-tier inspection queueing system. A queueing analysis will be demonstrated in Section III. Besides, we are going to derive the computing formulas for the steady-state probability and performance indices of the proposed queueing system. In Section IV, we will give an illustrative example to show and explain a step-by-step process for the presented computing method in a practical application. In Section V, we will conduct a series of case studies on the proposed queueing system. Through a series of numerical experiments, we figure out the effects on the system performance when the model parameters are varied, and reveal the managerial insights into the multi-tier inspection queueing system. Finally, the concluding remarks and suggestions are summarized in Section VI.

II. A MULTI-TIER QUEUEING MODEL WITH FINITE APPROVED CAPACITY

In this section, as shown in Fig. 1, we introduce a queueing system with multi-tier inspection channels, each with a multiple number of inspectors (with equipment). In order to understand the queueing impacts on inspecting the approved cross-border travelers, we will formulate a multi-tier queueing model with limited capacity (namely, pre-approval quantity) based on a health risk screening mechanism, and determine the performance measures of interests for the proposed multi-tier queueing system. In the studied multi-tier inspection queueing system, multiple risk thresholds are to be used to distinguish those approved cross-border travelers for going through differentiated tier of inspection channel. Based on the initial perceived risk level (assessed in the prescreening stage), we assign each approved traveler to a risk group, and then calibrates the inspection and quarantine measures to mitigate the risk associated with each risk group.

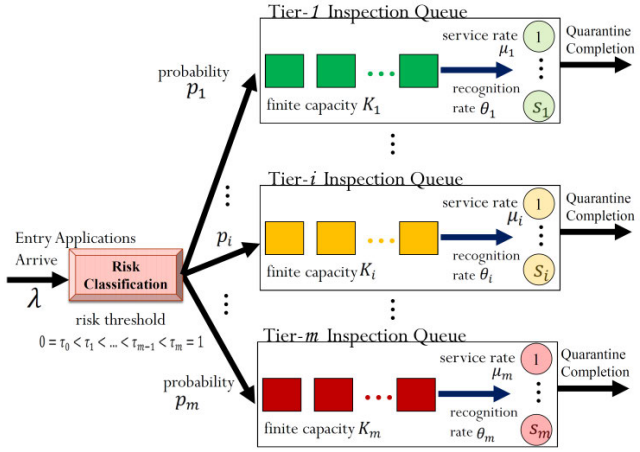

FIGURE 1. A multi-tier inspection queueing system with finite capacity.

We assume that the population of potential cross-border travelers is infinite, and the applications of travelers arrive to the border-crossing inspection and quarantine system according to a Poisson process with rate λ. In this study, we assume that the arriving travelers must be assigned to m approved risk classes, and we denote the index set $\mathbf{I} = \{1, 2, \ldots, m\}$ for the multiple risk classes. The queueing process for inspecting those approved cross-border travelers is divided into multiple levels of risk classification with probability p_i, for each class $i \in \mathbf{I}$.

Every cross-border traveler can be marked a risk value α (provided by a health risk pre-screening information system), and then will be inspected at the corresponding tier of inspection queue at the border checkpoints, where the risk value α is a real number and lies between 0% and 100%. We assume that the risk value α of cross-border travelers to be inspected follows a probability density function $f(\alpha)$, and the risk value of each traveler is independent of each other. In practice, the actual value of α could be estimated from the collected data sets, including the cumulative infectious cases, the number of close contacts, the number of quarantined individuals, geographic location, and so on. Besides, according to the historical data, the mathematical formulation of probability function $f(\alpha)$ could be derived by several statistical techniques, such as regression analysis, curve fitting, machine learning methods [29], etc.

We use the risk thresholds τ_i, for each $i \in \mathbf{I}$, to distinguish the adjacent levels of risk for those approved cross-border travelers. The values of risk thresholds τ_i for all $i \in \mathbf{I}$ are real numbers between zero and one, and the value range is set as $0 = \tau_0 < \tau_1 < \ldots < \tau_{m-1} < \tau_m = 1$. According to the assigned risk value α, the inspection officers will guide the approved cross-border travelers to be inspected in the corresponding tier of inspection channel.

Given the risk thresholds $0 = \tau_0 < \tau_1 < \ldots < \tau_{m-1} < \tau_m = 1$, the probability that the travelers are assigned to the i-th tier inspection channel can be derived as:

$$p_i = \int_{\tau_{i-1}}^{\tau_i} f(\alpha) d\alpha, \tag{1}$$

for each $i \in \mathbf{I}$. Note that, by the law of total probability, it is obvious that the following condition holds:

$$\sum_{i=1}^{m} p_i = 1. \tag{2}$$

Suppose that the service times (including inspection and quarantine) for approved travelers follow the exponential distributions, and the expected service time for the i-th tier of inspection channel is denoted as $1/\mu_i$, for each class $i \in \mathbf{I}$. Note that the m-th tiered inspection channel for the highest level of risk has the longest inspection time and strictest quarantine, whereas the first tiered inspection channel for the lowest level of risk has the shortest inspection time and the highest service efficiency. Meanwhile, for each class $i \in \mathbf{I}$, we represent s_i as the number of inspectors (with inspection and quarantine equipments) assigned to the i-th tier of inspection channel, where these numbers s_i are positive integers. Besides, it is also assumed that cross-border travelers are screened and inspected on a First-Come-First-Served basis within each tier of inspection channel.

In the considered queueing system as shown in Fig. 1, we have a finite capacity denoted as K_i for approved travelers assigned to the i-th risk class such that the total number of cross-border travelers in the i-th tiered inspection channel (queueing plus those in service) is no more than K_i. Note that these numbers K_i are positive integers, and it is realistic to assume $K_i \geq s_i$, for all $i \in \mathbf{I}$.

Meanwhile, for each risk class $i \in \mathbf{I}$, the recognition rate (for inspection and quarantine) at the i-th tier inspection channel is denoted as β_i, which is a constant number between 0% and 100%. It is worth noting that, for the sake of screening cost and efficiency, we may use more expensive screening equipment and quarantine materials for higher tier of inspection channel. In such case, β_m is the highest recognition rate, and β_1 is the lowest recognition rate.

The above-mentioned model assumptions are reasonable because the formulation of our queueing model comes from a new phenomenon in border control during the implementation of Travel Health Certificate/Passport for reopening international travel. In this scenario, before departure, travelers need to apply for the finite entry approval and then present their Travel Health Certificate (or COVID-19 vaccine certificate). Several countries, such as China, Japan and the European Union, have carried out such tests for innovative border control measures with finite capacity planning. Besides, the Travel Bubble between Taiwan and Palau is another practical example with the consideration of finite capacity planning under the current epidemic prevention and control.

In Table 1, we summarize the mathematical notations and definitions of the presented queueing model.

In the next subsection, we are going to formulate a multi-tier queueing model based on a multi-level inspection and quarantine procedure, which can be applied to evaluate trade-offs across multiple criteria in the checkpoints at borders, such as safety level, average number of travelers to be

TABLE 1. Notations for the multi-tier inspection queueing system.

Notation	Definition
$\mathbf{I}$	Index set for the risk class $i = 1, 2, \ldots, m-1, m$.
λ	The average arrival rate of cross-border travelers to be inspected.
α	The risk value of travelers to be inspected, which is a random variable between 0% and 100%.
τ_i	The risk threshold for distinguishing i -th and $(i+1)$ -th risk classes of travelers, for each $i = 0, 1, \ldots, m-1, m$.
μ_i	The average service rate at the i-th tier inspection channel, for each class $i \in \mathbf{I}$.
s_i	The number of inspectors at the i-th tier inspection channel, for each class $i \in \mathbf{I}$.
p_i	The probability of travelers assigned to the i-th tier inspection channel, for each class $i \in \mathbf{I}$.
K_i	The finite capacity for approved travelers at the i-th tier inspection channel, for each class $i \in \mathbf{I}$.
β_i	The recognition rate for inspection and quarantine at the i -th tier inspection channel, which is a constant number between 0% and 100%, for each class $i \in \mathbf{I}$.
R_i	The risk ratio of approved travelers at the i-th tier inspection channel, for each class $i \in \mathbf{I}$.
Performance Index of the Queueing System	
D_i	The rejection rate of travelers' applications to the i-th tier inspection channel, for each class $i \in \mathbf{I}$.
L	The average number of travelers at the overall multi-tier queueing system.
W	The average sojourn time spent by a traveler at the overall multi-tier queueing system.
R	The safety level of the overall multi-tier queueing system.

inspected, average sojourn time, and utilization level of the system.

III. A QUEUEING ANALYSIS

A. COMPUTATION FOR STEADY-STATE PROBABILITY

We denote $q_i(t)$ as the total number of cross-border travelers (in service or waiting) in the i-th tier of inspection channel at time t, for each class $i \in \mathbf{I}$. Since the arrival process of cross-border travelers to the inspection system is Poisson and the service times of multi-tier inspection channel are exponential, it can be observed that the stochastic process $\{(q_1(t), q_2(t), \ldots, q_m(t)), t \geq 0\}$ is a continuous time Markov chain. Besides, the state space of $\{(q_1(t), q_2(t), \ldots, q_m(t)), t \geq 0\}$ is finite because the queue lengths, $q_1(t) \leq K_1, q_2(t) \leq K_2, \ldots,$ and $q_m(t) \leq K_m$ are finite.

Since the independence of arrivals and the memoryless property of the exponential service time distribution, it implies that the counting number of cross-border travelers to be inspected at the i-th tier of inspection channel forms a birth and death process with finite states $\{0, 1, \ldots, K_i\}$, for each class $i \in \mathbf{I}$. That is, for each class $i \in \mathbf{I}$, the stochastic process $\{q_i(t) | t \geq 0\}$ is a birth-death process with birth parameters

$$\lambda_{i,j} = \begin{cases} p_i \cdot \lambda, & \text{for } j = 0, 1, \ldots, K_i - 1, \\ 0, & \text{otherwise}, \end{cases} \tag{3}$$

and death parameters

$$\mu_{i,j} = \begin{cases} j \cdot \mu_i, & \text{for } j = 1, 2, \ldots, s_i, \\ s_i \cdot \mu_i, & \text{for } j > s_i + 1, \ldots, K_i, \end{cases} \tag{4}$$

when a fixed number s_i of inspectors (with equipment) are available in the i-th tier of inspection channel. It is easy to see that the number undergoing the inspection service at the i-th tier of inspection channel is $\min\{q_i(t), s_i\}$, and the number waiting for service is $\max\{q_i(t) - s_i, 0\}$.

Next, for each class $i \in \mathbf{I}$, we assume that there exists the steady-state occupancy probabilities of n $(0 \leq n \leq K_i)$ approved travelers, $\pi_{i,n}$. Let

$$\pi_{i,n} = \lim_{t \to \infty} \Pr\{q_i(t) = n\}, \text{ for } n = 0, 1, \ldots, K_i, \tag{5}$$

be the equilibrium distribution of queue length in the i-th tier of inspection channel. Besides, for the simplicity of derivation, we can use a notation ρ_i to represent the traffic intensity of the i-th tier of inspection channel for each class $i \in \mathbf{I}$.

Definition 1: The *traffic intensity* of the i-th tier of inspection channel is defined as the fraction of the time in which this tier of inspection channel is occupied, for all class $i \in \mathbf{I}$. That is, the average occupancy of the i-th tier of inspection channel is formulated as

$$\rho_i = \frac{p_i \cdot \lambda}{s_i \cdot \mu_i}, \tag{6}$$

where λ is the average arrival rate, p_i is the probability of travelers assigned to the i-th tier inspection channel, s_i is a fixed number of inspectors, and μ_i is the average service rate, for each class $i \in \mathbf{I}$.

For the i-th tier of inspection channel, for all $i \in \mathbf{I}$, the unique steady-state probability can be determined by the following iterative relation

$$\pi_{i,n} = \begin{cases} \frac{(S_i \cdot \rho_i)^n}{n!} \cdot \pi_{i,0}, & \text{for } n = 1, \ldots, S_i, \\ \frac{S_i^{S_i} \cdot \rho_i^n}{S_i!} \cdot \pi_{i,0}, & \text{for } n = S_i + 1, \ldots, K_i, \end{cases} \tag{7}$$

Solving for $\pi_{i,0}$ in the equation $\sum_{n=0}^{K_i} \pi_{i,n} = 1$, we can derive that

$$\pi_{i,0} = \left(\sum_{j=0}^{s_i - 1} \frac{(s_i \cdot \rho_i)^j}{j!} + \sum_{j=s_i}^{K_i} \frac{s_i^{s_i} \cdot \rho_i^j}{s_i!} \right)^{-1}, \quad \forall i \in \mathbf{I}. \tag{8}$$

Therefore, with the help of probability $\pi_{i,0}$, we can recursively determine the remainder probability $\pi_{i,n}$, for $n = 1, \ldots, K_i$, by means of the equation (7).

The steady-state probabilities $\pi_{i,n}$, for $n = 0, \ldots, K_i$, and for all $i \in \mathbf{I}$, can demonstrate the limiting behavior of the studied multi-tier queueing system. In the following, we are

going to determine the performance indices of interest by using the obtained steady-state probabilities, that is, the rejection rate D_i for each class $i \in \mathbf{I}$, the average sojourn time W, the average number L, and the safety level R of the studied multi-tier queueing system.

B. PERFORMANCE INDEX OF THE QUEUEING SYSTEM

For each class $i \in \mathbf{I}$, when the queue of the i-th tier of inspection channel is full, all new applications of travelers for entry in the i-th risk class will be blocked. As a result, in the case of occupancy $n = K_i$, we can derive the rejection rate

$$D_i = \frac{s_i^{s_i} \cdot \rho_i^{K_i}}{s_i!} \cdot \left\{ \sum_{j=0}^{s_i-1} \frac{(s_i \cdot \rho_i)^j}{j!} + \sum_{j=s_i}^{K_i} \frac{s_i^{s_i} \cdot \rho_i^j}{s_i!} \right\}^{-1}, \tag{9}$$

for each risk class $i \in \mathbf{I}$, by using the equations (7) and (8).

Proposition 1: For all class $i \in \boldsymbol{I}$, it holds that the rejection rate of the i-th tier of inspection channel is decreasing with respect to the finite capacity for approved travelers at the i-th tier inspection channel. Namely, as we increase the capacity K_i, the rejection rate D_i will be decreased, for each class $i \in \boldsymbol{I}$.

Proposition 2: Given that the finite capacity K_i and the number of inspectors s_i are fixed, it holds that the rejection rate of the i-th tier of inspection channel is increasing with respect to the traffic intensity at the i-th tier inspection channel, for all class $i \in \boldsymbol{I}$. That is, the rejection rate D_i is an increasing function of the traffic intensity ρ_i, for each class $i \in \boldsymbol{I}$.

Next, we can evaluate the average queue length in the i-th tier of inspection channel, L_i, and the average number of approved travelers in the overall queueing system, L, by using the obtained steady-state probabilities. In the long term, the average queue length of the i-th tier of inspection channel can be derived as

$$\begin{aligned} L_i &= \sum_{n=0}^{K_i} n \cdot \pi_{i,n} \\ &= \left(\sum_{n=1}^{s_i} \frac{(s_i \cdot \rho_i)^n}{(n-1)!} + \sum_{n=s_i+1}^{K_i} \frac{n \cdot s_i^{s_i} \cdot \rho_i^n}{s_i!} \right) \cdot \pi_{i,0} \\ &= \left(\sum_{n=1}^{s_i} \frac{(s_i \cdot \rho_i)^n}{(n-1)!} + \sum_{n=s_i+1}^{K_i} \frac{n \cdot s_i^{s_i} \cdot \rho_i^n}{s_i!} \right) \\ &\quad \cdot \left(\sum_{j=0}^{s_i-1} \frac{(s_i \cdot \rho_i)^j}{j!} + \sum_{j=s_i}^{K_i} \frac{s_i^{s_i} \cdot \rho_i^j}{s_i!} \right)^{-1} \end{aligned} \tag{10}$$

for all risk class $i \in \mathbf{I}$. Using the explicit expression of the average queue length L_i, we can define the percentage of the average occupancy with respect to the maximum occupancy as follows.

Definition 2: Given the finite capacity K_i and the average queue length L_i, the *utilization level* of the i-th tier of inspection channel is defined as

$$U_i = \frac{L_i}{K_i}, \tag{11}$$

for all class $i \in \mathbf{I}$.

Proposition 3: For all class $i \in \boldsymbol{I}$, it holds that the average queue length of the i-th tier of inspection channel is increasing with respect to the finite capacity for approved travelers at the i-th tier inspection channel. Namely, if the traffic intensity ρ_i and the number of inspectors s_i are fixed, then the average queue length L_i is an increasing function of the capacity K_i, for each class $i \in \boldsymbol{I}$.

Proposition 4: The average queue length L_i is increasing in the traffic intensity ρ_i, and the upper bound of the average queue length L_i is the finite capacity K_i, given that the number of inspectors s_i and the capacity K_i are fixed, for each class $i \in \boldsymbol{I}$.

After determining the average queue length L_i, we can derive the expected number of approved travelers to be inspected in the whole system. Therefore, in the long run, the average number of approved travelers in the overall multi-tier queueing system can be determined as

$$\begin{aligned} L &= \sum_{i=1}^{m} p_i \cdot L_i = \sum_{i=1}^{m} p_i \cdot \pi_{i,0} \\ &\quad \cdot \left(\sum_{n=1}^{s_i} \frac{(s_i \cdot \rho_i)^n}{(n-1)!} + \sum_{n=s_i+1}^{K_i} \frac{n \cdot s_i^{s_i} \cdot \rho_i^n}{s_i!} \right), \end{aligned} \tag{12}$$

where p_i is the predetermined probability that the incoming travelers are assigned to the i-th tier inspection channel, and the values of steady-state probability $\pi_{i,0}$ for all risk class $i \in \mathbf{I}$ can be computed by using the equation (8).

Due to the limited capacity for approved travelers assigned to every differentiated risk class, the effective arrival rate to each tier of inspection channel can be obtained via the rejection rate D_{i} derived in the equation (9) as follows:

$$\lambda_i^{\text{effective}} = \lambda \cdot p_i \cdot (1 - D_i), \tag{13}$$

for all risk class $i \in \mathbf{I}$. Next, with the help of Little's formula, we can determine the average sojourn time spent by an approved traveler assigned to the i-th tier inspection channel via the following formula:

$$W_i = \frac{L_i}{\lambda_i^{\text{effective}}} = \frac{L_i}{\lambda \cdot p_i \cdot (1 - D_i)}, \tag{14}$$

for all risk class $i \in \mathbf{I}$. Therefore, in the long term, the average sojourn time spent for passing through the overall multi-tier queueing system can be determined as follows:

$$W = \sum_{i=1}^{m} p_i \cdot W_i = \sum_{i=1}^{m} p_i \cdot \frac{L_i}{\lambda \cdot p_i \cdot (1 - D_i)}, \tag{15}$$

where p_i is the predetermined probability that the incoming travelers are assigned to the i-th tier inspection channel for all risk class $i \in \mathbf{I}$.

Furthermore, under the given risk thresholds $0 = \tau_0 < \tau_1 < \ldots < \tau_{\mathrm{m}-1} < \tau_{\mathrm{m}} = 1$, we can derive the risk ratio of the cross-border travelers assigned to the i-th tier inspection channel, for each risk class $i \in \mathbf{I}$, as follows:

$$R_i = \frac{\int_{\tau_{i-1}}^{\tau_i} \alpha \cdot f(\alpha) d\alpha}{\int_0^1 \alpha \cdot f(\alpha) d\alpha}, \tag{16}$$

where $f(\alpha)$ is a probability density function of the risk value α for those approved travelers to be inspected. Therefore,

from the condition (2), we can determine the safety level of the overall multi-tier inspection system as follows:

$$R = \sum_{i=1}^{m} \beta_i \cdot R_i, \tag{17}$$

where β_i is the recognition rate for inspection and quarantine at the corresponding i-th tier inspection channel, which is a constant number between 0% and 100%. For the highest risk class, m, we use the most expensive screening equipment and quarantine materials with the highest recognition rate β_m. However, in consideration of shortage of inspection and quarantine resources, we may use the cheaper screening equipment and quarantine materials in the lower tier of inspection channel, which results in the lower recognition rate. In such case, β_1 is the lowest recognition rate due to the use of the cheapest screening equipment and quarantine materials for the lowest tier of inspection channel.

In summary, from the equation (9), we obtain the first performance index for the overall multi-tier inspection queueing system, that is, the rejection rate D_i of travelers' applications to the i-th tier inspection channel, for each class $i \in \mathbf{I}$. Next, through the calculation of formula (12), we can determine the second performance index, L, which represents the average number of approved travelers inspected at the overall multi-tier queueing system. Thirdly, by using the equation (15), we calculate the average sojourn time spent for passing through the overall multi-tier queueing system, W. Finally, we can determine the fourth performance index for the overall multi-tier inspection queueing system, the safety level R, by means of the formula (17).

IV. AN ILLUSTRATIVE EXAMPLE

In this section, we introduce a step-by-step process for the proposed computing method through solving an illustrative example. In practical applications, we can input the model parameters and probability density functions according to the real-time statistical data for solving the studied multi-tier inspection queueing model.

As an illustrative example taken from [2], it is given that the risk value α of the travelers to be inspected follows a truncated exponential distribution, and each risk value is independent of each other. The probability density function of a truncated exponential distribution is given as follows:

$$f(\alpha|\theta) = \frac{e^{-\alpha/\theta}}{\theta(1 - e^{-1/\theta})}, 0 < \alpha \leq 1, \tag{18}$$

where θ is the parameter of the truncated exponential distribution. Therefore, the average risk value $E[\alpha]$ of travelers to be inspected can be expressed as follows:

$$E[\alpha] = \int_0^1 \alpha \cdot f(\alpha|\theta)\, d\alpha = \theta - \frac{e^{-1/\theta}}{1 - e^{-1/\theta}} \approx \theta. \tag{19}$$

That is, the average risk value $E[\alpha]$ is approximately the parameter θ of the truncated exponential distribution.

From equation (1), given the risk thresholds $0 = \tau_0 < \tau_1 < \ldots < \tau_{m-1} < \tau_m = 1$, we can derive the probability that those cross-border travelers are to be assigned to the i-th tier of inspection channel as follows:

$$p_i = \int_{\tau_{i-1}}^{\tau_i} f(\alpha|\theta)\, d\alpha = \frac{e^{-\tau_{i-1}/\theta} - e^{-\tau_i/\theta}}{1 - e^{-1/\theta}}, \tag{20}$$

for each class $i \in \mathbf{I}$. In addition, with the help of equation (6), we can easily determine the traffic intensity of the i-th tier of inspection channel, ρ_i, for all $i \in \mathbf{I}$. Thus, by means of equations (7) and (8), we can recursively determine the steady-state probabilities $\pi_{i,n}$, for $n = 0, \ldots, K_i$, and for all $i \in \mathbf{I}$.

After obtaining the above steady-state probabilities, we can calculate the performance indices of interest by using equations (9), (12), and (15). For example, the average rejection rate D for the whole multi-tier queueing system is computed as follows:

$$D = \sum_{i=1}^{m} p_i \cdot D_i, \tag{21}$$

where D_i is the rejection rate determined by means of equation (9) for each class $i \in \mathbf{I}$. Next, the average number L for the whole queueing system can be estimated from the equation (12), and the average sojourn time W for the whole multi-tier queueing system can be determined with the formula (15).

Furthermore, from the equation (16), we can derive the risk ratio of the cross-border travelers assigned to the i-th tier inspection channel as follows:

$$\begin{aligned} R_i &= \frac{\int_{\tau_{i-1}}^{\tau_i} \alpha \cdot f(\alpha) d\alpha}{\int_0^1 \alpha \cdot f(\alpha) d\alpha} \\ &= \frac{\tau_i \cdot e^{-\tau_i/\theta} + \theta \cdot e^{-\tau_i/\theta} - \tau_{i-1} \cdot e^{-\tau_{i-1}/\theta} - \theta \cdot e^{-\tau_{i-1}/\theta}}{e^{-1/\theta} + \theta \cdot e^{-1/\theta} - \theta}, \end{aligned}$$

for each risk class $i \in \mathbf{I}$. Hence, by using the equation (17), we can estimate the average safety level $R = \sum_{i=1}^{m} \beta_i \cdot R_i$ for the studied multi-tier queueing system.

V. SENSITIVITY ANALYSIS

In this section, we conduct a sensitivity analysis on the studied queueing system through a series of numerical experiments to figure out the effects of varying model parameters on the system performance. Besides, those study cases in the following subsections could be potential applications for the differentiated service for inspection and quarantine during the global post-COVID economic recovery.

Our computational experiments are conducted with the software MATLAB R2014b on Windows 10 Professional 64-bit with the processor Intel (R) Core (TM) i7-6500U CPU@2.50GHz dual-core and 8 GB memory.

A. A UNIFORM INSPECTION QUEUEING SYSTEM

In this study case as $m = 1$, we show that our multi-tier inspection queueing model can be simplified to a uniform inspection system with only one type of inspection channels, where everyone is treated with identical inspection and quarantine procedures. For most countries/areas, the current

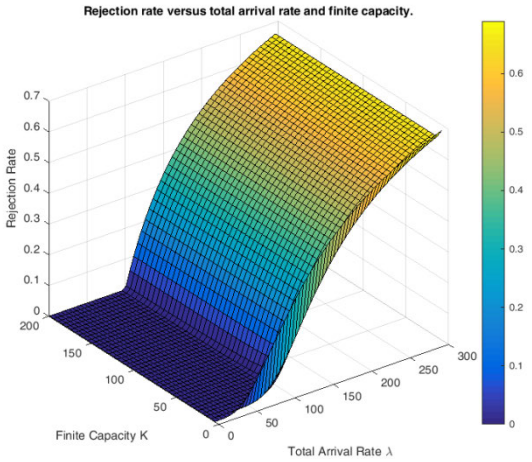

FIGURE 2. A 3D diagram for the average rejection rate D versus total arrival rate λ and finite capacity K, when implementing the uniform inspection procedure (a case as $m = 1$).

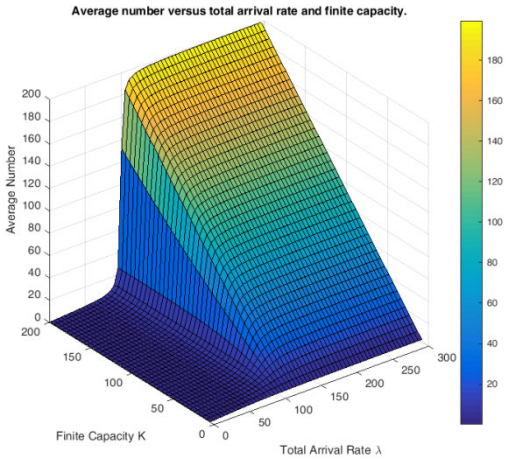

FIGURE 3. A 3D diagram for the average number L versus total arrival rate λ and finite capacity K, when implementing the uniform inspection procedure (a case as $m = 1$).

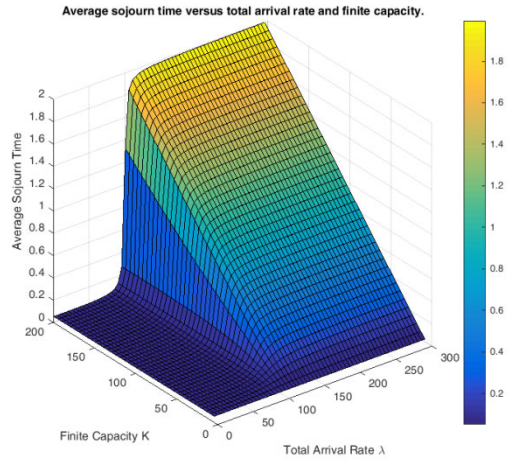

FIGURE 4. A 3D diagram for the average sojourn time W versus total arrival rate λ and finite capacity K, when implementing the uniform inspection procedure (a case as $m = 1$).

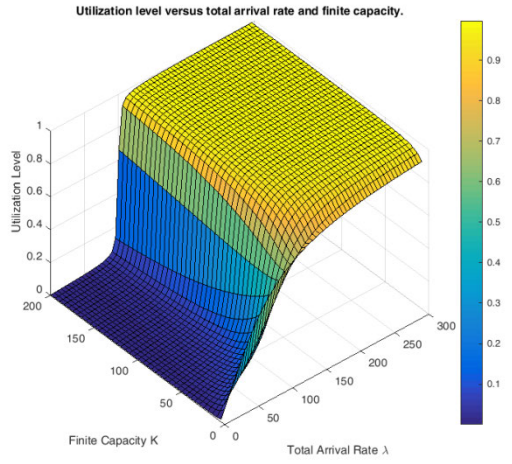

FIGURE 5. A 3D diagram for the average utilization level U versus total arrival rate λ and finite capacity K, when implementing the uniform inspection procedure (a case as $m = 1$).

epidemic prevention and control tasks are to uniformly apply the same inspection, quarantine and isolation procedures to all travelers, and hence, subject all travelers to the same level of risk and cost.

The parameter settings of this uniform inspection queueing system are given as follows. The average arrival rate can be observed from $\lambda = 1$ (traveler per day) to $\lambda = 300$ (travelers per day). The number of inspectors (with equipments) set is given as $s = 5$ (inspectors), and the finite capacity in this uniform inspection system can be set from $K = 5$ (travelers) to $K = 200$ (travelers). Meanwhile, the average service rate for each inspector is set as $\mu = 20$ (travelers/day).

When we vary the total arrival rate λ and finite capacity K, the numerical results are visualized in several three-dimensional diagrams in Figures 2-5 to show the impact on those performance indices of interest, such as the average rejection rate D, the average sojourn time W, the average number L, the average utilization level U. In Fig. 2, it illustrates that the average rejection rate is increasing in accordance to the total arrival rate, whereas the average rejection rate is decreasing to a stable value when increasing the finite capacity. In Fig. 3, it shows that the average number is increasing whether we increase the total arrival rate or the limited capacity. From the calculation of (14), we obtain the similar phenomenon for the average sojourn time when varying the total arrival rate and the finite capacity, as shown in Fig. 4. In Fig. 5, it indicates that the average utilization level is increasing in accordance to the total arrival rate, whereas there is no obvious monotone relationship between the average utilization level and the finite capacity.

Due to the shortages in medical capacity and resources to inspect the whole potential travelers, the uniform inspection has inevitably put isolation hotels or hospitals in vulnerable positions. Therefore, in the following subsections, we study a differentiated inspection strategy, that is, some travelers receive expedited inspecting whereas others receive enhanced inspecting.

B. A TWO-TIER INSPECTION QUEUEING SYSTEM

In this study case as $m = 2$, we show that our multi-tier inspection queueing model can be simplified to an inspection

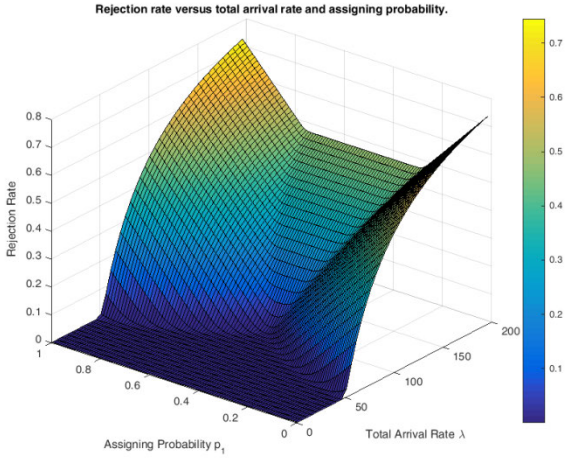

FIGURE 6. A 3D diagram for the average rejection rate D versus total arrival rate λ and assignment probability p_1, when the number of risk classes is set as $m = 2$.

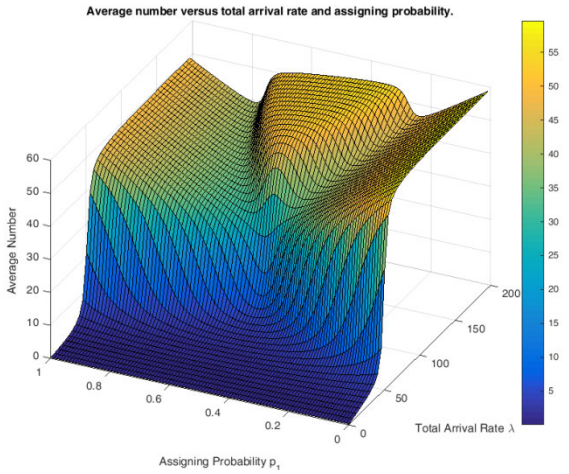

FIGURE 7. A 3D diagram for the average number L versus total arrival rate λ and assignment probability p_1, when the number of risk classes is set as $m = 2$.

queue with only two types of inspection channels and one risk threshold $0 \leq \tau_1 \leq 1$. In such a case, the proposed queueing model is reduced to a two-tier inspection queueing model consists of high-risk inspection channels (the second tier) and low-risk inspection channels (the first tier).

The parameter settings of this study case are given as follows: The total arrival rate is varied from $\lambda = 1$ (traveler per day) to $\lambda = 200$ (travelers per day). The numbers of inspectors with equipments set in this two-tier inspection system are given as $s_1 = 2$ (inspectors) and $s_2 = 5$ (inspectors), and the finite capacity for each tier of inspection channels is set as $K_1 = 50$ (travelers) and $K_2 = 60$ (travelers). Meanwhile, the recognition rates are given as $\beta_1 = 80\%$ and $\beta_2 = 99\%$. The average service rate for each tier of inspection channel is set as $\mu_1 = 26$ (travelers/day) and $\mu_2 = 10$ (travelers/day).

Besides, we also vary the assignment probability p_1 within the range of input values between 0 and 1. Here, the assignment probability p_1 represents the ratio of approved travelers to be assigned to the first tier inspection channel, and the ratio of approved travelers to be assigned to the other tier inspection channel is $(1-p_1)$. In this study case, we conduct several data analysis to understand the effects of varying the assignment probability because the assignment probability is one of the important factors affecting the system performance.

When we vary the total arrival rate $1 \leq \lambda \leq 200$ and assignment probability $0 \leq p_1 \leq 1$, the numerical results are visualized in the three-dimensional diagrams from Fig. 6 to Fig. 9. It can be observed in Fig. 6 that the average rejection rate is increasing when increasing the total arrival rate, whereas the average rejection rate is concave up in accordance to the finite capacity. In Fig. 7, it illustrates that the average number is increasing in accordance to the total arrival rate, whereas there is no obvious monotone relationship between the average number and the assignment probability. Similarly, in Fig. 8 and Fig. 9, we observe the same phenomenon for both the average sojourn time and the average utilization level.

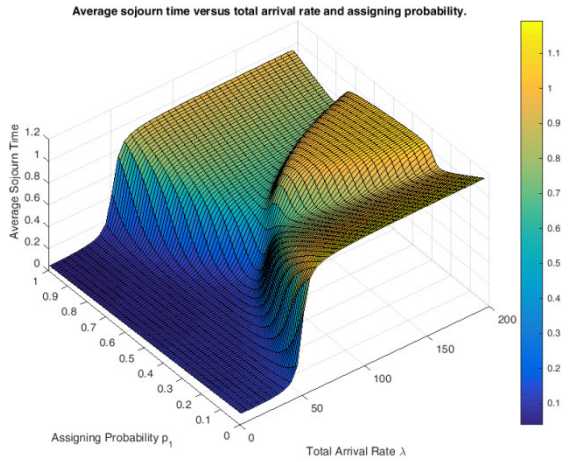

FIGURE 8. A 3D diagram for the average sojourn time W versus total arrival rate λ and assignment probability p_1, when the number of risk classes is set as $m = 2$.

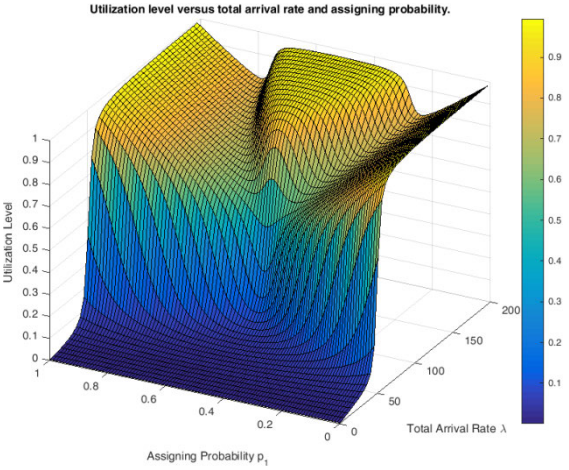

FIGURE 9. A 3D diagram for the average utilization level U versus total arrival rate λ and assignment probability p_1, when the number of risk classes is set as $m = 2$.

Next, we also investigate the effects of varying the input value of risk threshold τ_1. Because there is only one risk

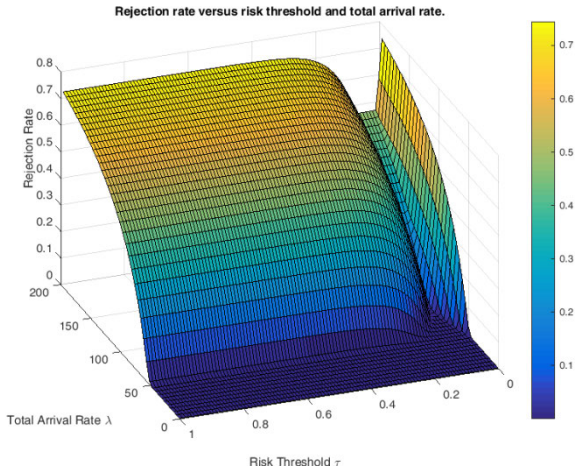

FIGURE 10. A 3D diagram for the average rejection rate D versus the risk threshold τ_1 and total arrival rate λ, when the number of risk classes is set as $m = 2$ and the probability density function $f(\alpha)$ for the risk value α of cross-border travelers is given as (18).

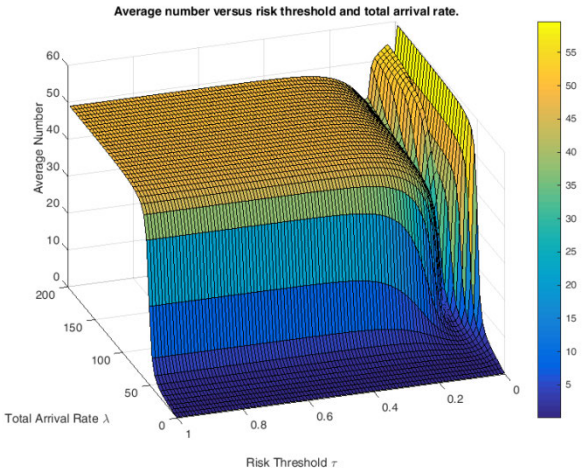

FIGURE 11. A 3D diagram for the average number L versus the risk threshold τ_1 and total arrival rate λ, when the number of risk classes is set as $m = 2$ and the probability density function $f(\alpha)$ for the risk value α of cross-border travelers is given as (18).

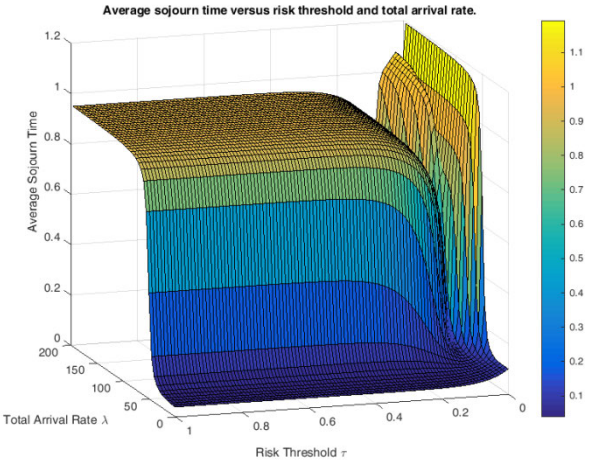

FIGURE 12. A 3D diagram for the average sojourn time W versus the risk threshold τ_1 and total arrival rate λ, when the number of risk classes is set as $m = 2$ and the probability density function $f(\alpha)$ for the risk value α of cross-border travelers is given as (18).

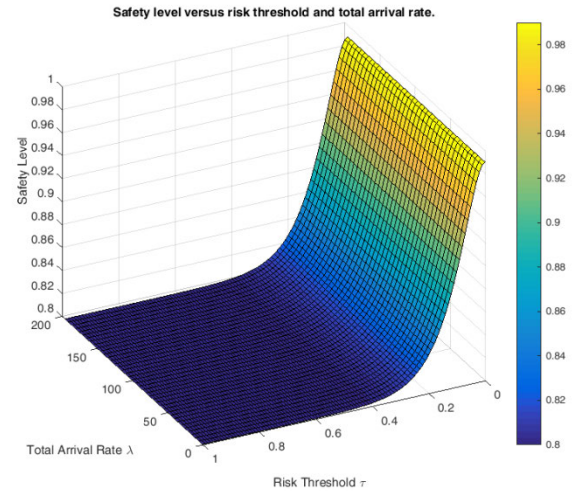

FIGURE 13. A 3D diagram for the average safety level R versus the risk threshold τ_1 and total arrival rate λ, when the number of risk classes is set as $m = 2$ and the probability density function $f(\alpha)$ for the risk value α of cross-border travelers is given as (18).

threshold used in this two-tier inspection queueing system, it is easier to provide a visualized illustration of the relationship between risk threshold and those performance indices of interest. Here, we assume that the probability density function $f(\alpha)$ for the risk value α of cross-border travelers is given as (18), and the risk threshold τ_1 is varied within the interval [0%, 100%], i.e., $0 \leq \tau_1 \leq 1$. In addition, we take $\theta = 0.0625$ as the input parameter of truncated exponential distribution in the following numerical experiments. Hence, when a value of risk threshold τ_1 is given, we can compute the assignment probabilities p_1 and p_2 through the equation (20). Those numerical results are depicted in the three-dimensional diagrams from Fig. 10 to Fig. 14.

In Fig. 10, it illustrates that the average rejection rate is increasing in accordance to the total arrival rate. However, the average rejection rate could be decreasing within a certain range of risk threshold values, and then the average rejection rate would increase to a stable value when increasing the risk threshold. In Fig. 11, it shows that the average number is increasing in accordance to the total arrival rate, whereas there is a complex relationship between the average number and the risk threshold within a certain range of risk threshold values. Besides, in Fig. 12 and Fig. 14, we also observe that both the average sojourn time and the average utilization level increase monotonically with the total arrival rate, whereas neither the average sojourn time nor the average utilization level do not change monotonically with increasing risk threshold values. However, it can be found in Fig. 13 that the average safety level is decreasing monotonically in accordance to the risk threshold, and there is no relationship between the average safety level and the total arrival rate.

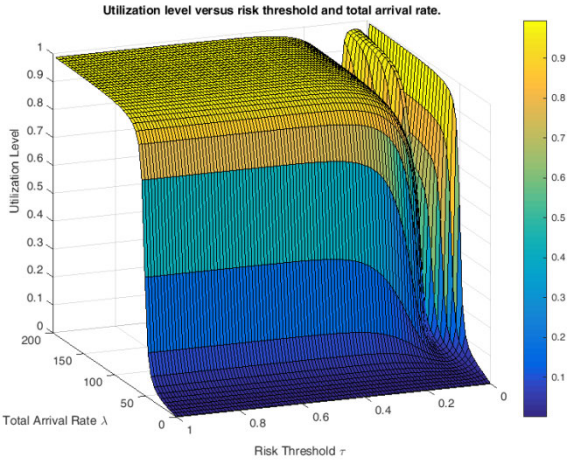

FIGURE 14. A 3D diagram for the average utilization level U versus the risk threshold τ_1 and total arrival rate λ, when the number of risk classes is set as $m = 2$ and the probability density function $f(\alpha)$ for the risk value α of cross-border travelers is given as (18).

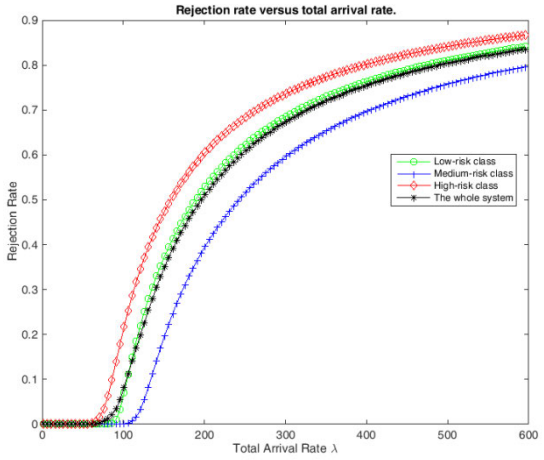

FIGURE 15. A diagram for the average rejection rate D versus total arrival rate λ, when the number of risk classes is set as $m = 3$.

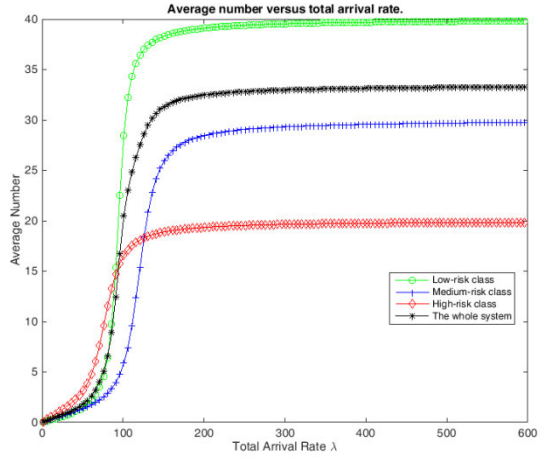

FIGURE 16. A diagram for the average number L versus total arrival rate λ, when the number of risk classes is set as $m = 3$.

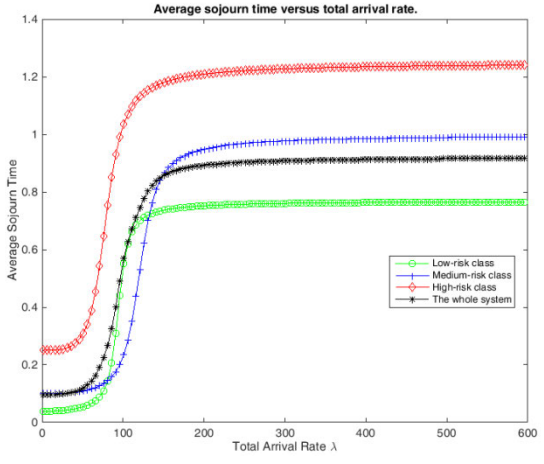

FIGURE 17. A diagram for the average sojourn time W versus total arrival rate λ, when the number of risk classes is set as $m = 3$.

C. A THREE-TIER INSPECTION QUEUEING SYSTEM

In this study case as $m = 3$, it represents a three-tier inspection queueing system consists of low-risk inspection channel (the first tier), medium-risk inspection channel (the second tier), and high-risk inspection channel (the third tier). Meanwhile, there are two risk thresholds $0 \le \tau_1 < \tau_2 \le 1$ in the studied model, which are used to distinguish those cross-border travelers for going through differentiated tier of inspection channels.

Here, the parameter settings are given as follows. The total arrival rate is varied from $\lambda = 1$ (traveler per day) to $\lambda = 600$ (travelers per day). The numbers of inspectors with equipments are set as $s_1 = 2$ (inspectors), $s_2 = 3$ (inspectors), and $s_3 = 4$ (inspectors), and the finite capacity for each tier of inspection channels is set as $K_1 = 40$ (travelers), $K_2 = 30$ (travelers), and $K_3 = 20$ (travelers). Meanwhile, the recognition rates are given as $\beta_1 = 80\%$, $\beta_2 = 90\%$, and $\beta_3 = 99\%$. The average service rates are set as $\mu_1 = 26$ (travelers/day), $\mu_2 = 10$ (travelers/day), and $\mu_3 = 4$ (travelers/day). Here, we assume that the probability density function $f(\alpha)$ for the risk value α of cross-border travelers is given as (18), and two risk thresholds $\tau_1 = 0.05$ and $\tau_2 = 0.1$ are fixed. Meanwhile, we take $\theta = 0.0625$ as the input parameter of truncated exponential distribution in the following numerical experiments.

When we vary the total arrival rate λ, the sensitivity analysis for those performance indices are illustrated as follows. In Fig. 15, it illustrates that the average rejection rates D and D_i, for all classes $i = 1, 2, 3$, are increasing monotonically with increasing arrival rate. Similarly, when increasing the total arrival rate, we find that the average number, the average sojourn time and the average utilization level are increasing monotonically for the whole system and all risk classes, which can be observed in Fig. 16, Fig. 17 and Fig. 19.

In Fig. 18, it shows that the average safety level R and three risk ratios R_i, for $i = 1, 2, 3$, do not change with increasing arrival rate. The reason why the average safety level and three risk ratios remain constant values is that those two risk thresholds are fixed in this example. In practice,

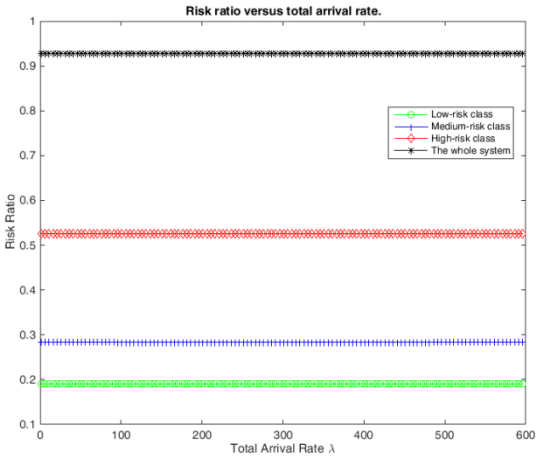

FIGURE 18. A diagram for the average safety level R and the risk ratio R_i versus total arrival rate λ, when the number of risk classes is set as $m = 3$.

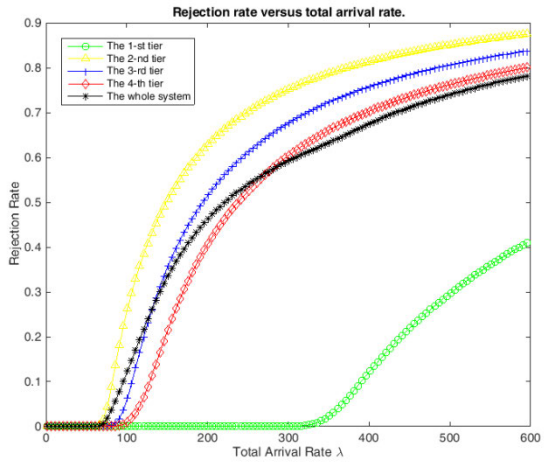

FIGURE 20. A diagram for the average rejection rate D versus total arrival rate λ, when the number of risk classes is set as $m = 4$.

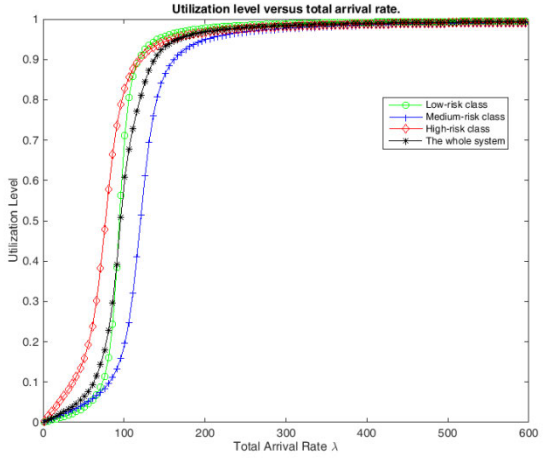

FIGURE 19. A diagram for the average utilization level U versus total arrival rate λ, when the number of risk classes is set as $m = 3$.

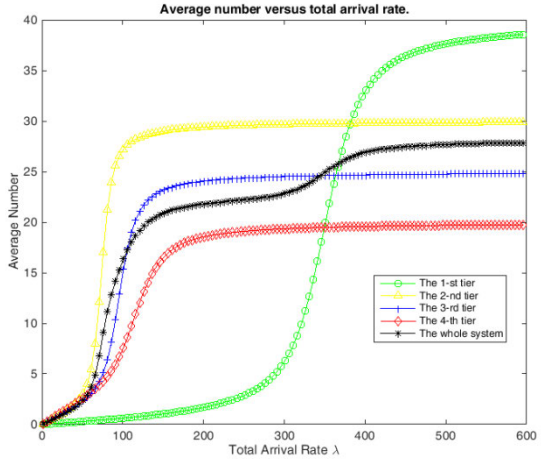

FIGURE 21. A diagram for the average number L versus total arrival rate λ, when the number of risk classes is set as $m = 4$.

when inputting different values of those two risk thresholds, we can easily determine the average safety level and three risk ratios by using the equations (1) and (16). For example, when two risk thresholds $\tau_1 = 0.05$ and $\tau_2 = 0.1$ are given, we can determine the assignment probabilities $p_1 = 55.07\%$, $p_2 = 24.74\%$, and $p_3 = 20.19\%$ by means of equation (1). Besides, we can estimate three risk ratios $R_1 = 19.12\%, R_2 = 28.39\%$ and $R_3 = 52.49\%$ by using equation (16). Therefore, the average safety level is computed as $R = \sum_{i=1}^{3} \beta_i \cdot R_i = 92.81\%$.

D. A FOUR-TIER INSPECTION QUEUEING SYSTEM

In this study case as $m = 4$, it represents a four-tier inspection queueing system consists of three risk thresholds $0 \leq \tau_1 < \tau_2 < \tau_3 \leq 1$. Here, the probability density function $f(\alpha)$ is given as (18) with a parameter $\theta = 0.0625$, and three risk thresholds $\tau_1 = 0.01$, $\tau_2 = 0.05$ and $\tau_3 = 0.1$ are fixed. Besides, the numbers of inspectors with equipments are set as $s_1 = 2$ (inspectors), $s_2 = 3$ (inspectors), $s_3 = 4$ (inspectors), and $s_4 = 6$ (inspectors), and the finite capacity for each tier of inspection channels is set as $K_1 = 40$ (travelers), $K_2 = 30$ (travelers), $K_3 = 25$ (travelers), and $K_4 = 20$ (travelers). Meanwhile, the recognition rates are given as $\beta_1 = 80\%$, $\beta_2 = 90\%$, $\beta_3 = 97\%$, and $\beta_4 = 99\%$. The average service rates are set as $\mu_1 = 26$ (travelers/day), $\mu_2 = 10$ (travelers/day), $\mu_3 = 6$ (travelers/day), and $\mu_4 = 4$ (travelers/day).

When we vary the total arrival rate from $\lambda = 1$ (traveler per day) to $\lambda = 600$ (travelers per day), those performance indices of the studied queueing system are depicted from Fig. 20 to Fig. 24. Firstly, in Fig. 20, it illustrates that the average rejection rates for the whole system and four risk classes are increasing monotonically with increasing arrival rate. Next, in Fig. 21, Fig. 22 and Fig. 24, it can be observed that the average number, the average sojourn time and the average utilization level are increasing monotonically when we increase the total arrival rate.

In Fig. 23, it shows that the average safety level and four risk ratios do not change when we vary the total arrival rate. The reason is that those risk thresholds are fixed in this

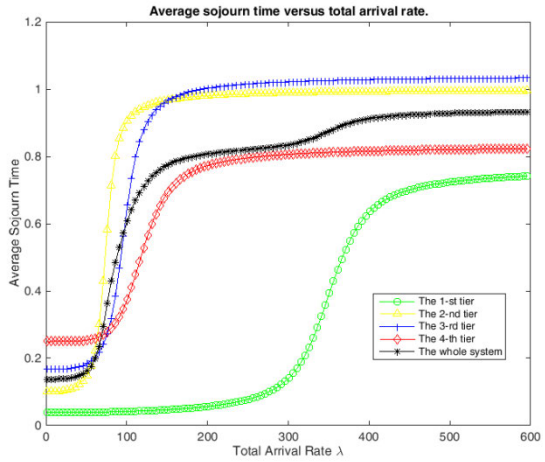

FIGURE 22. A diagram for the average sojourn time W versus total arrival rate λ, when the number of risk classes is set as $m = 4$.

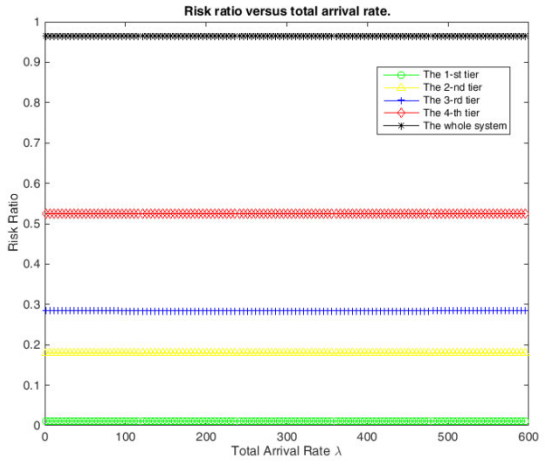

FIGURE 23. A diagram for the average safety level R and the risk ratio R_i versus total arrival rate λ, when the number of risk classes is set as $m = 4$.

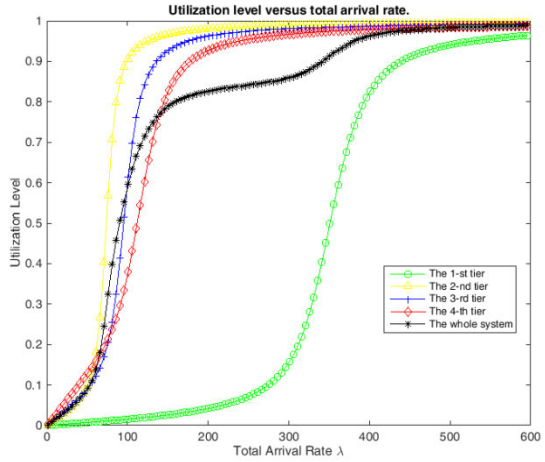

FIGURE 24. A diagram for the average utilization level U versus total arrival rate λ, when the number of risk classes is set as $m = 4$.

illustrative example. If the decision makers input different values of those three risk thresholds in their scenarios, we still can determine the corresponding values of the average safety level and four risk ratios by using the equations (1) and (16). From equation (1), we can determine the assignment probabilities $p_1 = 14.79\%$, $p_2 = 40.28\%$, $p_3 = 24.74\%$, and $p_4 = 20.19\%$, when three risk thresholds $\tau_1 = 0.01$, $\tau_2 = 0.05$ and $\tau_3 = 0.1$ are given. Besides, we can estimate three risk ratios $R_1 = 1.15\%$, $R_2 = 17.97\%$, $R_3 = 28.39\%$, and $R_4 = 52.49\%$ by using the equation (16). Therefore, we can obtain the average safety level $R = \sum_{i=1}^{4} \beta_i \cdot R_i = 96.60\%$.

VI. CONCLUSION

With the global strengthening of epidemic management and the continuous increase of the proportion of COVID-19 vaccination, we have stepped into the post epidemic era. Differentiated inspection and quarantine measures can reduce the risk of infected travelers entering the border without uniform isolation measures. In order to meet the needs of all kinds of travel bubbles and public health corridors, our work can be applied in formulating feasible inspection measures for hierarchical diversion in the cross-border flow of travelers. The computing method and plenty of data analysis presented in this paper can help the governments improve the operational efficiency of inspection and quarantine service while reducing the risk of virus entering their borders.

Based on a differentiated risk classification mechanism, we studied a multi-tier inspection queueing system with finite capacity for inspecting cross-border travelers, and demonstrated a computational method to evaluate the system performance. The steady-state probability of the proposed queueing model was derived in the paper to demonstrate the long-term behavior of the system. Besides, several mathematical formulas were also obtained for the performance indices of interest by means of the determined steady-state probability, such as the rejection rate of approved travelers, the average number of travelers to be inspected, the average sojourn time spent by each traveler, the utilization level and the safety level for the whole queueing system.

A series of numerical experiments were conducted in this work for the data analysis of the studied system. In the sensitivity analysis, we figured out the relationship between model parameters and system performance. Meanwhile, it provided a more detailed understanding of the derived formulas and the trade-off between safety and efficiency in the operational process of the queueing system. The contribution of data analysis is to provide the visualization for managerial insight into the structure and characteristics of the proposed queueing model, which can help decision makers update the existing inspection process or develop a new scheme dynamically according to the change of statistical data.

In the future works, it would be possible to supplement our queueing model with the additional waiting pool having an infinite buffer, where all rejected travelers could be re-addressed (once or many times) for service. In this

potential application, the healthy traveler rejected due to full capacity can be re-assigned to another tier of inspection channels if the original inspection channel is full. Besides, it would also be possible to derive mathematical analysis for such extension of our model by applying the matrix analytical methods.

During the global economic recovery, our findings in this paper could help the decision makers improve the current inspection and quarantine mechanism, under consideration of both strengthening supervision and optimizing service for inspection and quarantine. For different types of international travelers with hierarchical risk levels, we can carry out the risk assessment by classification or stratification. The queueing analysis in our research could be a useful reference for decision makers to scientifically evaluate and analyze the system performance and safety level. With the implementation of open and secure COVID-19 detection or vaccine information flow, we can verify the authenticity of the tests/vaccines and the identity of the person who presents the health certificate/passport. Therefore, the presented queueing model would be widely used in practical applications when providing differentiated service that take both risk and efficiency into account, such as the relaxation of access restrictions on theme parks, stadiums, and rail stations, etc.

REFERENCES

[1] V. Chamola, V. Hassija, V. Gupta, and M. Guizani, "A comprehensive review of the COVID-19 pandemic and the role of IoT, drones, AI, blockchain, and 5G in managing its impact," *IEEE Access*, vol. 8, pp. 90225–90265, 2020, doi: 10.1109/ACCESS.2020.2992341.

[2] C.-H. Wang, "A three-level health inspection queue based on risk screening management mechanism for post-COVID global economic recovery," *IEEE Access*, vol. 8, pp. 177604–177614, 2020, doi: 10.1109/ACCESS.2020.3026786.

[3] Y. Shen, D. Guo, F. Long, L. A. Mateos, H. Ding, Z. Xiu, R. B. Hellman, A. King, S. Chen, C. Zhang, and H. Tan, "Robots under COVID-19 pandemic: A comprehensive survey," *IEEE Access*, vol. 9, pp. 1590–1615, 2021, doi: 10.1109/ACCESS.2020.3045792.

[4] World Health Organization (WHO). *Coronavirus disease (COVID-19) Pandemic*. Accessed: Mar. 14, 2021. [Online]. Available: https://www.who.int/emergencies/diseases/novel-coronavirus-2019

[5] L. A. Albert, A. Nikolaev, A. J. Lee, K. Fletcher, and S. H. Jacobson, "A review of risk-based security and its impact on TSA PreCheck," *IISE Trans.*, vol. 53, no. 6, pp. 657–670, Jun. 2021, doi: 10.1080/24725854.2020.1825881.

[6] *Transportation Security Administration of the United States of America (TSA)*. TSA checkpoint travel numbers for 2020 and 2019. Accessed: Jan. 20, 2021. [Online]. Available: https://www.tsa.gov/coronavirus/passenger-throughput

[7] International Air Transport Association (IATA). *IATA Travel Pass for Travelers*. Accessed: Jan. 28, 2021. [Online]. Available: https://www.iata.org/en/youandiata/travelers/iata-travel-pass-for-travelers/

[8] V. L. Lazar Babu, R. Batta, and L. Lin, "Passenger grouping under constant threat probability in an airport security system," *Eur. J. Oper. Res.*, vol. 168, no. 2, pp. 633–644, Jan. 2006.

[9] H. Cavusoglu, B. Koh, and S. Raghunathan, "An analysis of the impact of passenger profiling for transportation security," *Oper. Res.*, vol. 58, no. 5, pp. 1287–1302, Oct. 2010.

[10] A. G. Nikolaev, A. J. Lee, and S. H. Jacobson, "Optimal aviation security screening strategies with dynamic passenger risk updates," *IEEE Trans. Intell. Transp. Syst.*, vol. 13, no. 1, pp. 203–212, Mar. 2012.

[11] C.-H. Wang, "A modelling framework for managing risk-based checkpoint screening systems with two-type inspection queues," in *Proc. 3rd Int. Conf. Robot, Vis. Signal Process. (RVSP)*, Kaohsiung, Taiwan, Nov. 2015, pp. 220–223.

[12] C.-H. Wang, "Arena simulation for aviation passenger security-check systems," in *Genetic and Evolutionary Computing (Advances in Intelligent Systems and Computing)*, vol. 536. Cham, Switzerland: Springer, pp. 95–102, 2016.

[13] M. G. Stewart and J. Mueller, "Risk and economic assessment of expedited passenger screening and TSA PreCheck," *J. Transp. Secur.*, vol. 10, nos. 1–2, pp. 1–22, Jun. 2017.

[14] C. Song and J. Zhuang, "Modeling precheck parallel screening process in the face of strategic applicants with incomplete information and screening errors," *Risk Anal.*, vol. 38, no. 1, pp. 118–133, Jan. 2018.

[15] C.-H. Wang and X. Wu, "Performance analysis of a security-check system with four types of inspection channels for high-speed rail stations in China," in *Proc. Smart Service Syst., Oper. Manage., Anal. INFORMS Int. Conf. Service Sci. (ICSS)*, H. Yang, Ed. Nanjing, China: Springer, Jun. 2019, pp. 7–16.

[16] A. J. Lee and S. H. Jacobson, "The impact of aviation checkpoint queues on optimizing security screening effectiveness," *Rel. Eng. Syst. Saf.*, vol. 96, no. 8, pp. 900–911, Aug. 2011.

[17] Z. G. Zhang, H. P. Luh, and C.-H. Wang, "Modeling security-check queues," *Manage. Sci.*, vol. 57, no. 11, pp. 1979–1995, 2011.

[18] S. Wong and N. Brooks, "Evolving risk-based security: A review of current issues and emerging trends impacting security screening in the aviation industry," *J. Air Transp. Manage.*, vol. 48, pp. 60–64, Sep. 2015.

[19] C. Song and J. Zhuang, "Two-stage security screening strategies in the face of strategic applicants, congestions and screening errors," *Ann. Oper. Res.*, vol. 258, no. 2, pp. 237–262, Nov. 2017.

[20] C.-H. Wang, "A matrix-analytic method for evaluating performance of security-check system with two-type inspection queues," in *Proc. Int. Conf. Ind. Eng. Syst. Manage. (IESM)*, Shanghai, China, Sep. 25-27, 2019.

[21] Y. Deutsch and B. Golany, "Securing gates of a protected area: A hybrid game and queueing theory modeling approach," *Decis. Anal.*, vol. 16, no. 1, pp. 31–45, Mar. 2019.

[22] X. Nie, G. Parab, R. Batta, and L. Lin, "Simulation-based selectee lane queueing design for passenger checkpoint screening," *Eur. J. Oper. Res.*, vol. 219, pp. 146–155, May 2012.

[23] C.-H. Wang and H. P. Luh, "Estimating the loss probability under heavy traffic conditions," *Comput. Math. Appl.*, vol. 64, no. 5, pp. 1352–1363, Sep. 2012.

[24] H. Luh, Z. G. Zhang, and C.-H. Wang, "A computing approach to two competing services with a finite buffer effect," *Proc. 8th Int. Conf. Queueing Theory Netw. Appl. (QTNA)*, 2013, pp. 15–21.

[25] L. Lin, Q. Wang, and A. W. Sadek, "Border crossing delay prediction using transient multi-server queueing models," *Transp. Res. A: Policy Pract.*, vol. 64, pp. 65–91, Jun. 2014.

[26] C.-H. Wang, M.-E. Wu, and C.-M. Chen, "Inspection risk and delay for screening cargo containers at security checkpoints," in *Proc. Int. Conf. Intell. Inf. Hiding Multimedia Signal Process. (IIH-MSP)*, Adelaide, NSW, Australia, Sep. 2015, pp. 211–214.

[27] D. Amorim da Cunha, R. Macário, and V. Reis, "Keeping cargo security costs down: A risk-based approach to air cargo airport security in small and medium airports," *J. Air Transp. Manage.*, vol. 61, pp. 115–122, Jun. 2017.

[28] G. J. Hanumantha, B. T. Arici, J. A. Sefair, and R. Askin, "Demand prediction and dynamic workforce allocation to improve airport screening operations," *IISE Trans.*, vol. 52, no. 12, pp. 1324–1342, Dec. 2020.

[29] A. Andreas, C. X. Mavromoustakis, G. Mastorakis, S. Mumtaz, J. M. Batalla, and E. Pallis, "Modified machine learning techique for curve fitting on regression models for COVID-19 projections," in *Proc. IEEE 25th Int. Workshop Comput. Aided Modeling Design Commun. Links Netw. (CAMAD)*, Pisa, Italy, Sep. 2020, pp. 1–6.

CHIA-HUNG WANG (Member, IEEE) received the B.S. degree in mathematics from National Tsing Hua University, Hsinchu, Taiwan, in 2002, the M.S. degree in mathematical sciences from National Chengchi University, Taipei, Taiwan, in 2004, and the Ph.D. degree in operations research from the Department of Mathematical Sciences, National Chengchi University, in 2011.

He visited the University of Illinois at Chicago, USA, as a Visiting Scholar, from August 2007 to August 2008. From 2011 to 2015, he was a Postdoctoral Fellow with National Chiao Tung University and National Cheng Kung University, Taiwan. In 2015, he joined the Fujian University of Technology, China, as a Faculty Member, where he has served as a Research Fellow with the Fujian Provincial Key Laboratory of Big Data Mining and Applications. He currently holds an Associate Professor position at the College of Information Science and Engineering, Fujian University of Technology. He is an Expert in operations research, applied mathematics, information systems, and data science. He has been involved in several collaborative projects with international professionals, including the modeling and analysis of security-check queues, the management mechanisms for service systems, and the design of management schemes on communication networks. These research works have already been published in more than 60 refereed journals and conference proceedings, including *Management Science*, *Soft Computing*, *Computers and Operations Research*, IEEE Access, *Computers and Mathematics With Applications*, *International Journal of Information and Management Sciences*, and so on.

YU-TIN CHEN received the M.S. degree in genetics from National Yang Ming University, Taiwan, in 2000, and the Ph.D. degree in computer science from National Tsing Hua University, Taiwan, in 2012.

From 2000 to 2002, he was a Research Assistant with the Institute of Biochemistry, National Yang Ming University. From 2002 to 2004, he has served as a Research Associate with the Bioinformatics Division, Vita-Genomics Biotech Company, Taiwan. From 2012 to 2015, he has worked as a Postdoctoral Research Fellow with National Cheng Kung University, Taiwan. From 2015 to 2017, he has served as the Senior Manager of Genomics BioSci and Technology Company, Taiwan. From 2017 to 2019, he held a Senior Researcher position at the Biomedical Project of Yonglin Healthcare Foundation of Health Technology Business Group, Foxconn. He is currently the Founder and the CEO of Hengzen Technology Company Ltd., Taiwan, where he has been since 2019. He was involved in diverse academic and industrial projects, and achieved plenty of results in the field. He has authored or coauthored several peer-reviewed journals articles and conference papers, and holds two patents. His research interests include evolutionary genomics, comparative genomics, bio-sequence pattern visualization, NGS analysis, human gene information, network topology, and business in artificial intelligence. He guided the informatics pipeline in various platforms, such as the web services with database, which was the leading of blood cancer test in National Taiwan University Hospital, Taiwan.

XIAOJING WU was born in Fuzhou, Fujian, China, in 1982. She received the B.A. and M.S. degrees from Fujian Normal University, China, in 2004 and 2007, respectively. Since 2007, she has been a Lecturer with the Fujian University of Technology, China, where she currently holds a Lecturer position at the College of Electronics, Electrical Engineering and Physics. She hosted several research programs and published more than ten research articles. She is also the co-inventor of more than eight inventions. Her research interests include multiple-intelligences theory and applications, behavior science, and the comparative study of higher education.